Fraunhofer Institute
for Structural Durability and System Reliability LBF

InCeight Casting C^8

Proceedings of the 3rd Congress for Intelligent Combining of Design, Casting, Computer Simulation, Checking and Cyclic Behaviour for Efficient Cast Components, March 5th-6th, 2025, Darmstadt

Christoph Bleicher, Ahmad Qaralleh (eds.)

Fraunhofer Verlag

Contact:
Fraunhofer Institute
for Structural Durability and System Reliability LBF
Bartningstrasse 47
64289 Darmstadt
Germany
Phone +49 6151 705-0
info@lbf.fraunhofer.de
www.lbf.fraunhofer.de

Bibliographic information of the German National Library:
The German National Library has listed this publication in its Deutsche Nationalbibliografie; detailed bibliographic data is available on the internet at www.dnb.de.

ISBN: 978-3-8396-2083-0
ISSN: 2747-4895
DOI (free Open Access version): https://doi.org/10.24406/publica-4153

Print and finishing: Fraunhofer-Druckerei, Stuttgart

The book was printed with chlorine- and acid-free paper.

Nobelstraße 12
70569 Stuttgart
Germany
verlag@fraunhofer.de
www.verlag.fraunhofer.de

is a constituent entity of the Fraunhofer-Gesellschaft, and as such has no separate legal status.

Fraunhofer-Gesellschaft zur Förderung
der angewandten Forschung e.V.
Hansastraße 27 c
80686 München
Germany
www.fraunhofer.de

Determination of Local Fatigue Strength in Heavy-Section Castings using Simulative Synthetic S-N-Curves

Felix Weber, Victoria Schulz, Vitali Züch, Dennis Bosse, Georg Jacobs, Christoph Broeckmann

Abstract:
Modern wind turbines are a major success factor in the transformation towards renewable energies. Considering the increasing demand and power per turbine, the power density of modern wind turbines is continuously increasing. Thus, continuous optimization of the heavy-section ductile cast iron castings (e.g. torque arm, main shaft, or planet carrier) is conducted, and local utilization rates are increased.
A characteristic of such heavy-section castings is the local microstructure variation due to variations in the local solidification and cooling conditions. With local solidification and cooling conditions affecting the formation of graphite precipitates, matrix phases, matrix grain size distributions, and possible shrinkage formation, the resulting microstructure variations govern the mechanical properties. Due to the inherent statistical variance, the mechanical properties must also be interpreted in terms of statistical information.
However, significant leverage for local utilization rates is given by the consideration of local material properties such as fatigue strength. Considering the challenges of experimental testing of a specified microstructure state due to the reproducibility of statistically equivalent microstructures and mechanical testing, simulative testing concepts are required. This study provides an approach for determining the local fatigue strength in heavy-section castings by considering a multi-scale simulation model linking local microstructure and macroscopic loading.
The presented approach is based on a multi-scale fatigue initiation model. A macroscopic model determines the local load case within a complex geometry. A mesoscopic model based on a representative volume element (RVE) of the microstructure is linked with the macroscopic model using submodeling techniques. Within the mesoscopic model, the crack initiation under fatigue loading is determined using the Tanaka-Mura model, which links microcrack formation to the local dislocation accumulation on individual slip bands. For this physical modeling approach the local crack initiation energy and the critical resolved shear stress are required. Here, the crack initiation energy is a derivative of the J-integral solution, whereas the critical resolved shear stress is determined using micropillar compression tests.
Using this iterative multi-scale approach, simulative test results are determined for various load levels. As a result, the simulative synthetic S-N-curve is derived, and failure probabilities are estimated. The model's sensitivity to the microstructure is demonstrated by comparing different microstructure states associated with solidification and cooling conditions for thick and thin sections within a casting.

Keywords: Ductile Cast Iron, Fatigue Strength, Tanaka-Mura, Micromechanics, Representative Volume Element

1 Introduction

In the context of the shared societal goal of transitioning to a net zero energy system [1], the importance of wind turbines is continuously increasing. To account for this energy demand, the power of wind turbines is steadily increased, resulting in increased dimensions and weights of the used structural components, leading to challenges in manufacturing and logistics. Cast iron is taking a crucial role among the materials used for the heavy-weight structural components [2–4].
Among the required material properties, the fatigue strength is of substantial interest as it is required in strength assessment guidelines such as FKM [5] or DNVGL [6]. However, the determination of the local microstructure dependent fatigue strength within a heavy-section component is a fundamental problem for ductile cast iron grades used in structural

components such as solution strengthened ferritic ductile iron (SSF-DI) or ferritic ductile cast iron. This is due to the complex microstructure formation mechanism linked to the solidification and cooling behavior, which governs the formation of graphite precipitation, metallic matrix, and shrinkages [7].
With different solidification and cooling rates resulting in different sizes and morphologies of graphite precipitates and shrinkages, their influence on the fatigue strength for SSF-DI was shown by Gebhardt et al. [8–11] and Borsato et al. [12; 13] as well as for ferritic ductile cast iron by Benedetti et al. [14]. These macroscopically observed influences are supported by studies identifying the underlying micromechanisms: The formation of slip bands in the vicinity of graphite precipitates at local stress concentrations was observed for ferritic ductile cast iron by Bellini et [15]. In the case of SSF-DI Sujakhu et al. [16] and Gebhardt et al. [17] reported the same effect, whereas Gebhardt et al. [17] showed the dependence of slip band formation on the local ferrite orientation.
In order to give an estimate for the local microstructure dependent fatigue strength, Wu [18] showed the applicability of a modified Tanaka-Mura considering a local plastic strain definition indicating the local dislocation movement resulting in

$$N_\mathrm{f} = \frac{8(1-\nu)R_s w_s}{\mu b} \cdot \frac{1}{\Delta\gamma^2}$$

with N_f as number of load cycles for crack formation, ν the Poisson's ratio, R_s the surface roughness factor, w_s the surface energy, μ the shear modulus, b the Burgers vector, γ the equivalent shear strain [18]. Using a simulative model, Collini et al. [19; 20] presented a fatigue life prediction model for shrinkage defect evaluation using the virtual crack closure technique (VCCT). Gebhardt et al. [11] considered the Shakedown-Theorem for the high cycle fatigue strength estimation of SSF-DI. Here, a shakedown state is a state that has a total plastic dissipation that is bounded [21]. The influence of graphite precipitate morphology on the fatigue strength could be reproduced by Gebhardt et al. [9]. Considering the variety of approaches, there is, to the best of the author's knowledge, no holistic approach for the microstructure-based S-N-curve prediction of SSF-DI for the use as local material properties in modern strength assessment. This includes, in particular, a direct determination of finite life and fatigue strength within the high cycle fatigue regime based on a given microstructure or microstructure characteristics.
This study focuses on implementing a multi-scale fatigue initiation model for SSF-DI. Therefore, the Tanaka-Mura model is applied on a mesoscopic scale using two-dimensional representative volume elements and is linked to a macroscopic model representing the loading condition. A comparison of different microstructure states demonstrates the model's sensitivity towards local solidification and cooling conditions.

2 Material

The material investigated in this study is a heavy-section SSF-DI casting of grade EN-GJS-500-14. The material was cast in a sand mold by the foundry Silbitz Group Torgelow. A detailed material analysis is provided in [22]. 0 presents the change in local microstructure in dependence of the varying solidification and cooling conditions for cubes with wall thicknesses of 200 mm and 300 mm.

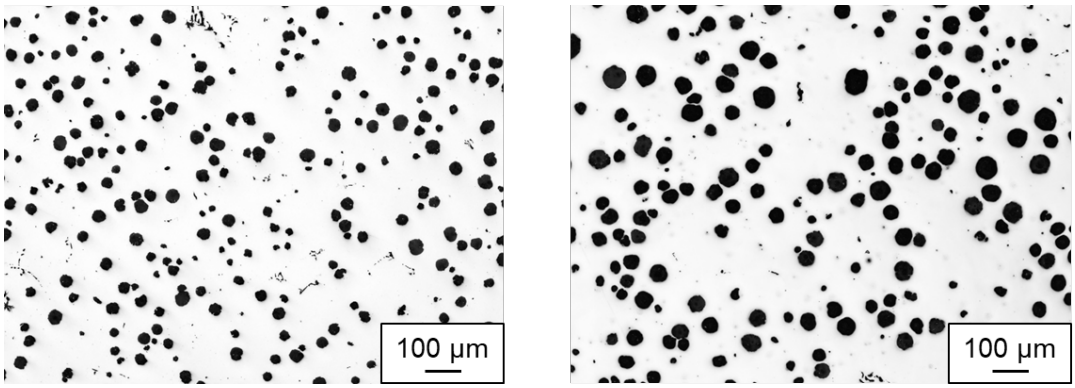

Fig. 1 Exemplary micrographs of the local microstructure in a 200 mm wall thickness (left) and 300 mm wall thickness (right) cast of the investigated SSF-DI EN-GJS-500-14.

Material samples from two distinct solidification and cooling conditions within the 200 mm and 300 mm cube associated with the local feedmod of 3.1 and 4.2 cm are taken as reference materials. Here, the feedmod is taken as a microstructure identifier since no feeders were used during casting and thus the feedmod is linked to the local solidification rate. For these material states, mechanical properties as a function of casting modulus have been determined in previous work [22]. Thus, the feedmod 3.1 cm can

be associated with an ultimate tensile strength of 473 MPa and a yield strength of 348 MPa [22]. Analogously, the feedmod of 4.2 cm can be correlated with an ultimate tensile strength and yield strength of 466 MPa and 345 MPa respectively [22].

3 Methodology

In the following, the concept of the multi-scale implementation of the Tanaka-Mura model, the RVE generation, and the model evaluation are described in detail.

3.1 The Tanaka-Mura Model for Fatigue Crack Initiation

The fundamental axiom of the presented model for SSF-DI is the shear stress induced local accumulation of dislocations in the ferritic matrix close to the graphite precipitates or shrinkages prior to crack initiation. According to the Tanaka-Mura model [23], a cyclic loading above the critical resolved shear stress (CRSS) τ_{CRSS} results in the local dipole dislocation accumulation on activated slip bands within a metallic grain. Within this model, the irreversibility of dislocation movement is considered, such that a continuous accumulation of stored energy occurs per load cycle [23]. Tanaka and Mura extended this theory toward crack initiation originating at a particle-matrix or void-matrix interface [24]. Considering the Tanaka-Mura model the stored energy increment ΔU due to dislocation accumulation per half loading cycle is

$$\Delta U = \frac{(\Delta\tau - 2\tau_{CRSS})^2 \pi a^2 (1-\nu)}{2G}$$

with $\Delta\tau$ as the locally acting shear stress, τ_{CRSS} as critical resolved shear stress, the shear modulus G, Poisson ratio ν, and $2a$ as grain diameter [24]. By combination with the required energy for crack initiation $4aW_c$ with W_c as crack initiation energy, the number of load cycles required for crack initiation can be calculated by

$$N_g = \frac{8GW_c}{\pi d(1-\nu)(\Delta\tau - 2\tau_{CRSS})^2}$$

with d as length of the crack [24]. Allowing the sequential crack growth within individual grains, Mlikota et al. [25] formulated a segment-based formulation of the Tanaka-Mura model as

$$N_s = \frac{8GW_c}{\pi d_s(1-\nu)(\Delta\tau - 2\tau_{CRSS})^2}$$

with d_s as length of a crack segment [25].

In the case of the fatigue crack initiation for SSF-DI, the model is used to describe the local dislocation movement within the ferritic grains under consideration of local stress concentrations due to graphite precipitates or shrinkages. With the ferritic matrix representing a body centered cubic crystal system, relevant slip systems could be identified as $\{1\,1\,0\}\langle 1\,1\,1\rangle$ [17]. For the application of the Tanaka-Mura model, the shear modulus G, the Poisson ratio ν, the critical shear stress CRSS, the local resolved shear stress $\Delta\tau$, the slip band length d_s, and the crack initiation energy W_c must be known. While shear modulus and Poisson ratio are well-known material parameters, the CRSS and crack initiation energy must be explicitly determined, e.g. by micropillar compression tests and interrupted fatigue tests.

The linkage of the formation of cracks according to the Tanaka-Mura model and the total fatigue lifetime of SSF-DI is based on the following axiom: The total lifetime of a material under fatigue loading can be split into two stages, namely, crack initiation and crack propagation. Here, crack initiation refers to the shear stress induced mode II crack formation mechanism. In contrast, crack propagation refers to the normal stress induced mode I crack formation mechanism. It is shown for metallic materials, that stage I crack initiation can account for up to 90 % of the total fatigue lifetime [26].

3.2 Multi-Scale Implementation of the Tanaka-Mura Model

A multiscale model consisting of a 3D continuous macroscopic specimen and a 2D mesoscopic representative volume element (RVE) is the basis of the FE model implemented in Abaqus, considering the concept introduced by Mlikota [25]. A flow chart of the simulation model is given in Fig. 2.

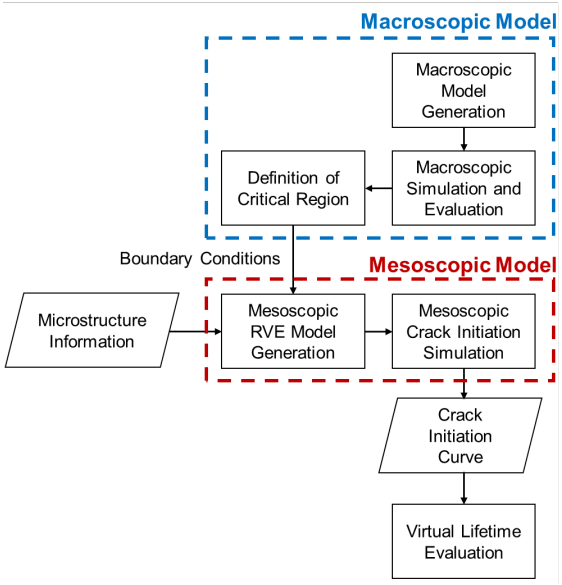

Fig. 2 Flow chart of the proposed multi-scale fatigue crack initiation simulation model.

Here, the macroscopic model is used to determine the displacements considered as boundary conditions within the mesoscopic model. The mesoscopic model determines the crack initiation according to the Tanaka-Mura model within the mesoscopic microstructure. Displacements are mapped from the macroscopic to the mesoscopic model using submodel boundary conditions by positioning the RVE close to the surface in the center of the testing region of the macroscopic model.
The complete simulation process, shown in 0, can be separated into three phases: model generation, simulation, and model evaluation.

Model Generation

The starting point of the simulation process is the model generation of the macroscopic and mesoscopic model. Here, the macroscopic model is derived from the considered specimen geometry (round notched specimen with a nominal diameter of 8 mm and a notch factor of 1.3) under consideration of homogeneous continuous material properties with tensile loads mimicking the upper stress amplitude for a stress ratio $\mathrm{R} = 0$ at the specimen heads as boundary conditions, comp. 0.

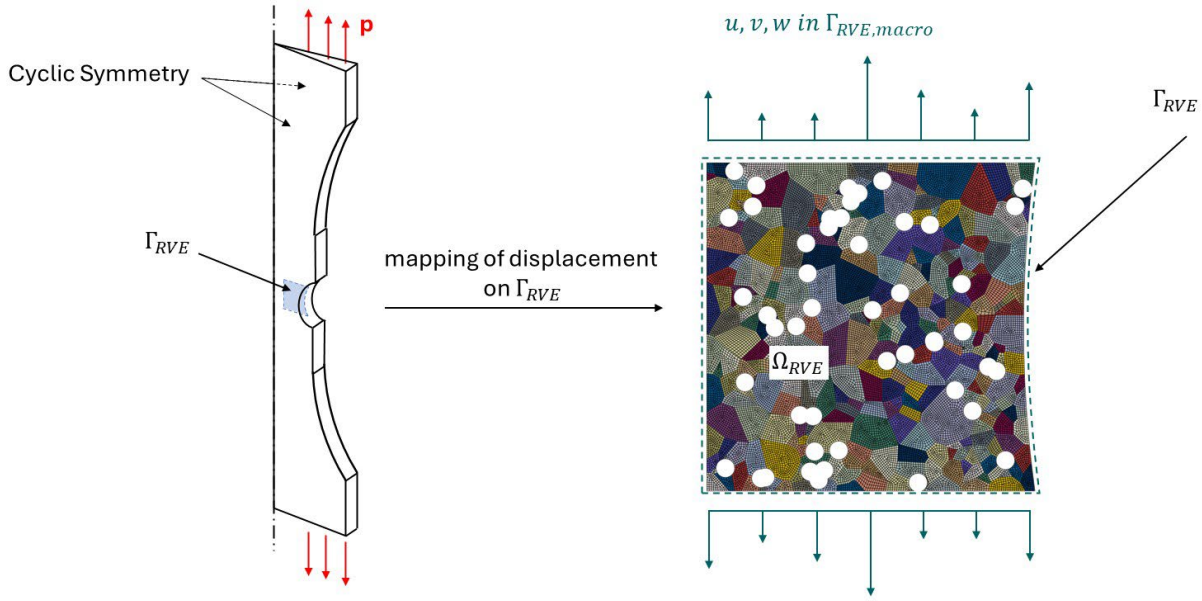

Fig. 3 Visualization of the interaction of the macroscopic and mesoscopic model in the proposed multi-scale model.

The mesoscopic model is an RVE of the SSF-DI with size 750 µm x 750 µm. Therefore, it considers information on the grain size distribution and the distribution of grain orientations, determined using electron backscatter diffraction (EBSD). Using Neper [27], the RVE model is generated through Voronoi tessellation and under consideration of grain-specific crystal orientations given as Euler angles. The grain interfaces are modeled as ideal without delamination. Subsequently, the generated ferritic grain matrix is modified by the insertion of pores mimicking graphite precipitates at the grain boundary triple junctions. Under consideration of the grain specific crystal orientations, the dominant slip bands and slip directions within the slip system $\{1\,1\,0\}\langle 1\,1\,1\rangle$ are calculated for each grain and split into five segments. Here, the dominant slip band refers to the slip bands with the highest Schmid factor under the applied external load that present the highest activation rate. Multiple slip bands are considered per each grain with a predefined slip band distance of 10 µm.

Iterative Fatigue Crack Initiation Simulation

Once the model has been created, the simulation step is carried out iteratively. A single iteration consists of stress field computation in the mesoscopic model, an update of slip band segment specific damage states, and the update of the geometric model. Using a linear-elastic quasi-static analysis, the resulting stress field is computed, and the stress tensors are linearly averaged along each slip band segment. The shear stress acting in slip direction for each slip band segment is calculated by projection of the linearly averaged stress tensor. For the total set of potentially activatable slip band segments the number of cycles to crack initiation is calculated according to the calculation scheme presented above. The slip band segment with the lowest number of cycles to crack initiation is considered as the “next-to-crack” slip band segment with N_{ntc} load cycles to failure and the damage state of all remaining slip band segments is incremented by the ratio N_{ntc}/N_{i} with N_{i} as the slip band segment specific load cycles to failure. The number of active slip bands per grain is limited to one such that all slip

band segments in the same grain as the "next-to-crack" slip band segment not belonging to the same slip band are deactivated. The mesoscopic model is updated by placing the cracked slip band segment as a crack seam within the geometric model and by opening the grain interfaces between two adjacent grains with activated slip band segments if the stress on the grain interface exceeds a von Mises stress of 414 MPa along the interface. Subsequently, the next iteration is started.

Model Evaluation

The goal of the model evaluation is to determine the transition from a global stage I mode II crack initiation to a stage II mode I crack propagation. Therefore, the crack propagation rate against the number of broken segments is considered, comp. 0.

Here, 4a presents a run-out specimen and 4b presents a failed specimen. Three characteristic regions can be seen in 0b: A – stage I mode II crack initiation, B – the transition of stage I to stage II, and C – stage II mode I crack propagation. The considered criterion for the end of stage I mode II crack initiation is reaching of the transition region B and a minimum crack length of the dominant crack within the mesoscopic model. Quantitatively, a run-out is characterized by a limited number of cracked slip band segments. For fractured specimens, the total lifetime is defined according to Mlikota [25], such that the end of mode II crack initiation is defined by the slip band segment, in which the number of load cycles to cracking exceeds seven times the average number of load cycles to cracking of the first then cracked slip band segments. The transition stage is marked in 0b.

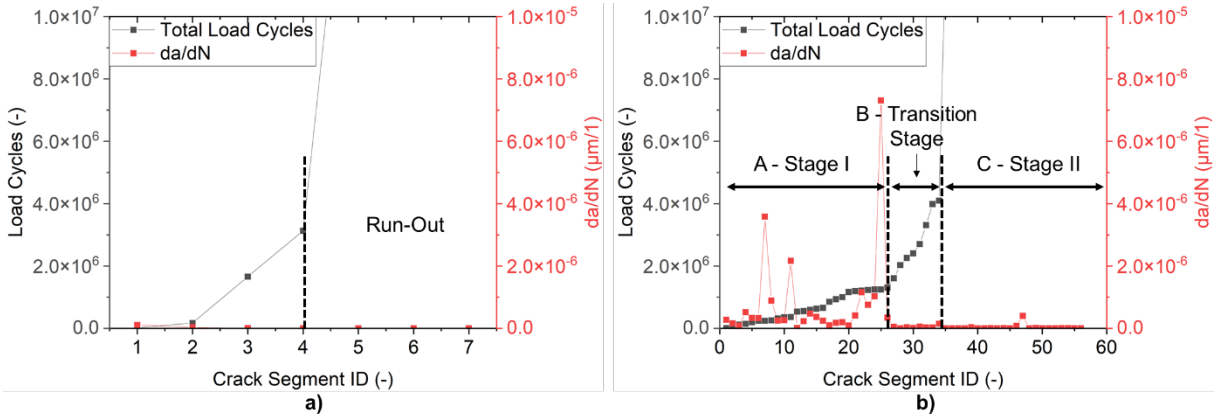

Fig. 4 a) Visualization of a run-out specimen, b) Visualization of crack propagation rate per cracked segment with three characteristic regions for a failed specimen: A – stage I mode II crack initiation, B – the transition of stage I to stage II, and C – stage II mode I crack propagation.

4 Results and Discussion

In the following, the simulative synthetic S-N-curves for the investigated two distinct microstructure states are shown and the model sensitivity is discussed.

The ferrite grain structure of the mesoscopic RVE for the feedmod 3.1 and 4.2 cm is generated based on EBSD analysis, resulting in lognormal distributions with $\mu = 3.23$ and $\sigma = 0.75$ and $\mu = 3.54$ and $\sigma = 0.79$, respectively. Here, ferrite grains with a diameter smaller than 10 µm are neglected. The inserted graphite precipitates follow the information given in 0. Two RVE were generated for each distinct solidification and cooling condition. Parameters considered in the Tanaka-Mura model are given in 0.

Tab. 1 Parameters considered for graphite precipitates during RVE generation.

Feedmod (cm)	Phase Fraction (%)	Number of Precipitates (-)	Precipitate Radius (µm)
3.1	12	48	21.27
4.2	12	42	22.72

Tab. 2 Parameters used in the Tanaka-Mura model for fatigue crack initiation evaluation

Parameter	Feedmod 3.1 cm	Feedmod 4.2 cm
Critical Resolved Shear Stress	136.3 MPa	136.3 MPa
Crack Initiation Energy	27.7 kJ/m^2	27.7 kJ/m^2

4.1 Simulative Synthetic S-N-curves

The initiated cracks within the mesoscopic model are exemplified in 0 for feedmod 4.2 cm and a load level of 157.5 MPa. Here, the microcracks form close to the surface and in the proximity of graphite precipitates due to local stress raising effects. However, crack initiation only occurs in preferably oriented grains. Thus, crack initiation does not occur at every graphite precipitate but only at those that present a preferably oriented ferrite grain in their proximity.

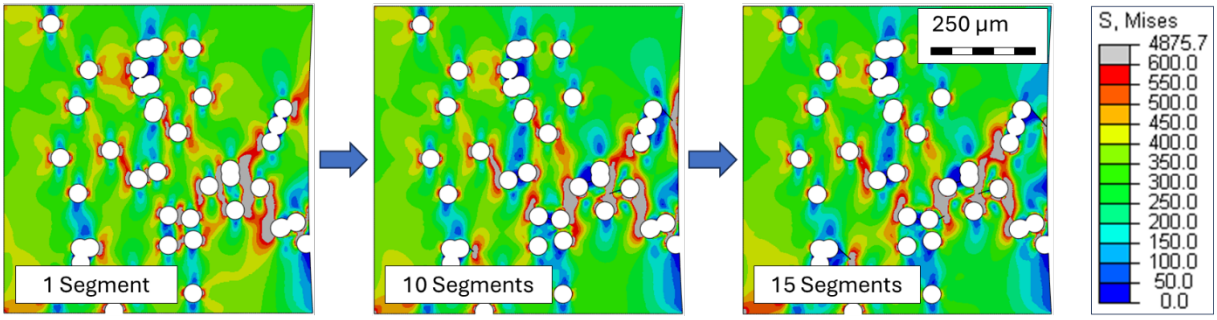

Fig. 5 Initiated fatigue cracks in the mesoscopic model of feedmod 4.2 cm for load level 157.5 MPa for iteration 1, 10, and 15 with associated cracked segments (left to right).

The resulting virtual fatigue testing points constructed using the model evaluation presented beforehand are shown in 0 for both investigated microstructure states. Using the virtual testing points in the finite life regime, simulative synthetic S-N-curves were constructed using the horizon method for the finite life regime. The resulting S-N-curves are shown in 0.

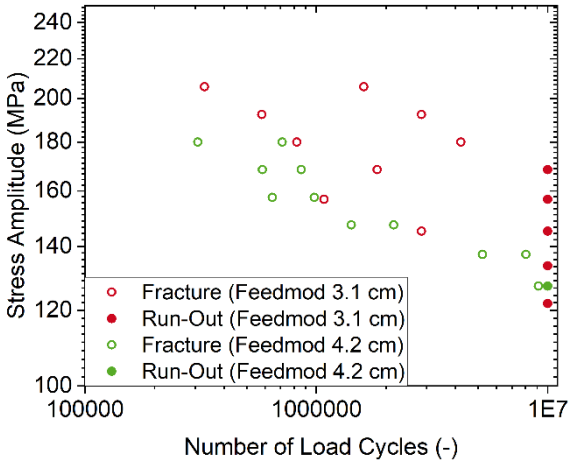

Fig. 6 Simulative fatigue test data points for the analyzed microstructure states of feedmod 3.1 and 4.2 cm.

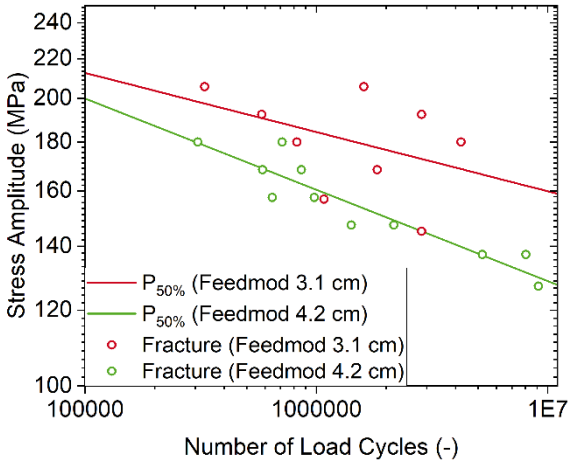

Fig. 7 Derived simulative S-N-curves for the analyzed microstructure states pf feedmod 3.1 and 4.2 cm.

Comparing the results for both microstructure states, one can see that the proposed approach is sensitive to the underlying microstructure in the RVE resulting in an increased fatigue strength for the faster solidification and cooling conditions. Considering the relatively small differences in graphite precipitate properties, a major influence on the fatigue strength is given by the underlying ferrite grain distribution. Here, faster solidification and cooling conditions result in a reduced ferrite grain size within the model leading to a strengthening of the material due to a higher number of grain interfaces acting as potential crack stoppers.

A comparison to the real properties of the investigated microstructure states can be achieved by consideration of the quasi-static mechanical

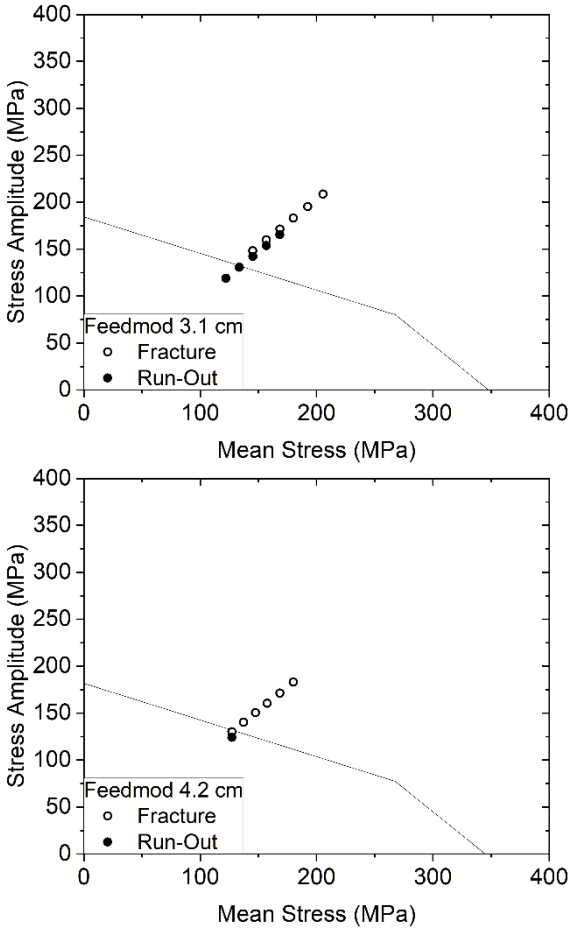

Fig. 8 Comparison of the virtual fatigue testing data to experimental data obtained in prior work [22] using Haigh diagrams constructed using the experimental data.

properties of prior works [22]Here, a Haigh diagram is constructed using the relationship of ultimate tensile strength and fatigue strength proposed by FKM [5], which states $\sigma_A = 0.39 \cdot R_m$ for the investigated SSF-DI grade EN-GJS-500-14. A combination of the resulting Haigh diagrams and the virtual fatigue data is presented in 0. Here, one can see a good agreement between the synthetic testing points and the estimate of the fatigue strength based on the Haigh diagram. Considering the significant influence of the model parameters critical resolved shear stress and crack initiation energy and the challenging determination of said parameters, the achieved results using the proposed multi-scale model approach are considered a feasible approach for the conduction of simulative fatigue tests. However, considering the limited available virtual fatigue testing data as of now, a detailed statistical analysis is required and will significantly enhance the evaluation of model applicability and the determination of validity bounds.

5 Conclusions and Outlook

This study presents a first simulative study of the fatigue crack initiation in SSF-DI EN-GJS-500-14 using a Tanaka-Mura based modeling approach. Therefore, a multi-scale fatigue crack initiation simulation was implemented, which linked a macroscopic fatigue specimen with an RVE used as a mesoscopic model. Within the mesoscopic model, microcrack initiation due to dislocation movement, according to the Tanaka-Mura model, was implemented. The used RVEs mimicked two distinct solidification and cooling conditions associated with 200 mm and 300 mm wall thicknesses. Based on the results, the model could depict the microstructure influence on the resulting fatigue strength. A comparison with prior experimental data resulted in good agreement. A distinct comparison of the modeling results indicated that the influence of the metallic matrix exceeds the influence of the modeled graphite precipitates.

Future work will be focused on the statistical validation of the presented results to allow for a clear definition of validity bounds for the presented model. Furthermore, the micromechanical model itself will be extended by the effect of concurrent slip system activation and silicon segregation within the microstructure affecting the local critical resolved shear stress. Transfer to component specific use-cases could be achieved by linkage to a subsequent XFEM analysis on the component scale, ultimately allowing for a closed simulation scheme for new component design procedures.

6 Acknowledgements

This research has been funded by the Federal Ministry for Economic Affairs and Climate Action (BMWK) in the project LeKoGussWEA under grant number 0324279A.

Supported by:

Federal Ministry
for Economic Affairs
and Climate Action

on the basis of a decision
by the German Bundestag

7 References

[1] International Energy Agency (2021) Net Zero by 2050: A Roadmap for the Global Energy Sector, 4th edn., Paris. https://www.iea.org/reports/net-zero-by-2050

[2] Shirani M, Härkegård G (2011) Large scale axial fatigue testing of ductile cast iron for heavy section wind turbine components, Trondheim. doi:10.1016/j.engfailanal.2011.05.005

[3] Weber F, Broeckmann C, Züch V, Jacobs G, Zimmermann J, Schröder K-U, Bami Y, Jakumeit J, Bodenburg M, Weiß R (2023) Multi-domain optimization of cast iron components in wind turbines. doi:10.1007/s10010-023-00616-3

[4] Dugic I (2013) Ductile iron for the wind power industry

[5] Forschungskuratorium Maschinenbau (2020) Rechnerischer Festigkeitsnachweis für Maschinenbauteile, 7th edn.

[6] Germanischer Lloyd (2010) DNVGL - Rules and Guidelines Industrial Services: Guideline for the Certification of Wind Turbines

[7] Wüllner E (2015) Einfluss von Legierungselementen auf die Gefügeausbildung und mechanische Eigenschaften von Gusseisen mit Kugelgraphit, Mönchengladbach

[8] Gebhardt C, Nellessen J, Bührig-Polaczek A, Broeckmann C (2021) Influence of Aluminum on Fatigue Strength of Solution-Strengthened Nodular Cast Iron. doi:10.3390/met11020311

[9] Gebhardt C, Chen G, Bezold A, Broeckmann C (2018) Influence of graphite morphology on static and cyclic strength of ferritic nodular cast iron. doi:10.1051/matecconf/201816514014

[10] Gebhardt C (2022) Einfluss der Graphitmorphologie auf die Langzeitfestigkeit von Gusseisen mit Kugelgraphit. Werkstoffanwendungen im Maschinenbau

[11] Gebhardt C, Trimborn T, Weber F, Bezold A, Broeckmann C, Herty M (2020) Simplified ResNet approach for data driven prediction of microstructure-fatigue relationship. doi:10.1016/j.mechmat.2020.103625

[12] Borsato T, Ferro P, Fabrizi A, Berto F, Carollo C (2021) Long solidification time effect on solution strengthened ferritic ductile iron fatigue properties. doi:10.1016/j.ijfatigue.2020.106137

[13] Borsato T, Ferro P, Berto F, Carollo C (2016) Mechanical and Fatigue Properties of Heavy Section Solution Strengthened Ferritic Ductile Iron Castings. doi:10.1002/adem.201600256

[14] Benedetti M, Fontanari V, Lusuardi D (2019) Effect of graphite morphology on the fatigue and fracture resistance of ferritic ductile cast iron. doi:10.1016/j.engfracmech.2018.12.019

[15] Bellini C, Di Cocco V, Favaro G, Iacoviello F, Sorrentino L (2019) Ductile cast irons: Microstructure influence on the fatigue initiation mechanisms. doi:10.1111/ffe.13100
[16] Sujakhu S, Castagne S, Sakaguchi M, Kasvayee KA, Ghassemali E, Jarfors A, Wang W (2018) On the fatigue damage micromechanisms in Si-solution–strengthened spheroidal graphite cast iron. doi:10.1111/ffe.12723
[17] Gebhardt C, Zhang J, Bezold A, Broeckmann C (2023) Microscale fatigue mechanisms in high silicon alloyed nodular cast iron. doi:10.1016/j.ijfatigue.2022.107402
[18] Wu X (2020) Microstructure-Fatigue Relationships for Cast Irons. doi:10.4271/2020-01-0187
[19] Collini L, Pirondi A (2014) Fatigue crack growth analysis in porous ductile cast iron microstructure. doi:10.1016/j.ijfatigue.2013.06.020
[20] Collini L, Pirondi A, Bianchi R, Cova M, Milella PP (2011) Influence of casting defects on fatigue crack initiation and fatigue limit of ductile cast iron. doi:10.1016/j.proeng.2011.04.481
[21] König J (1987) Shakedown of Elastic-Plastic Structures. https://www.sciencedirect.com/bookseries/fundamental-studies-in-engineering/vol/7/suppl/C
[22] Weber F, Züch V, Gebhardt C, Bezold A, Broeckmann C, Bosse D, Jacobs G, Gurevich V, Bodenburg M (2023) An Interdisciplinary Approach to Local Strength Assessment of Cast Iron Components to Exploit Unused Component Potential. doi:10.24406/publica-1036
[23] Tanaka K, Mura T (1981) A Dislocation Model for Fatigue Crack Initiation. doi:10.1115/1.3157599
[24] Tanaka K, Mura T (1982) A theory of fatigue crack initiation at inclusions. doi: 10.1007/bf02642422
[25] Mlikota M (2019) Multiscale modelling and simulation of metal fatigue and its applications. doi:10.18419/opus-11240
[26] Wang QY, Berard JY, Rathery S, Bathias C (1999) Technical note High-cycle fatigue crack initiation and propagation behaviour of high-strength sprin steel wires. doi:10.1046/j.1460-2695.1999.t01-1-00184.x
[27] Quey R, Dawson PR, Barbe F (2011) Large-scale 3D random polycrystals for the finite element method: Generation, meshing and remeshing. doi:10.1016/j.cma.2011.01.002

8 Authors

Bosse, Dennis
RWTH Aachen University, Center for Wind Power Drives (CWD), Aachen, Germany
Broeckmann, Christoph
RWTH Aachen University, Institut für Werkstoffanwendungen im Maschinenbau (IWM), Aachen, Germany
Jacobs, George
RWTH Aachen University, Center for Wind Power Drives (CWD), Aachen, Germany
Schulz, Victoria
RWTH Aachen University, Institut für Werkstoffanwendungen im Maschinenbau (IWM), Aachen, Germany
Weber, Felix
RWTH Aachen University, Institut für Werkstoffanwendungen im Maschinenbau (IWM), Aachen, Germany
Züch, Vitali
RWTH Aachen University, Center for Wind Power Drives (CWD), Aachen, Germany